

LASERS

PACS numbers: 42.55.Lt; 42.60.Lh
DOI: 10.1070/QE2006v036n02ABEH013109

Multisectional KrF laser with a pulse repetition rate of 4 kHz and inductive – capacitive discharge stabilisation

A.V. Andramanov, S.A. Kabaev, B.V. Lazhintsev,
V.A. Nor-Arevyan, A.V. Pisetskaya, V.D. Selemir

***Abstract*. An electric-discharge KrF laser with an inductive – capacitive discharge stabilisation and a pulse repetition rate up to 4 kHz is developed. The multisectional discharge gap with a total length of 25 cm is formed by 25 pairs of anode – cathode plates. A discharge width of no more than 1 mm is realised. Ne and He are used as the buffer gases, and F_2 serves as the fluorine donor. The maximum output pulse energy is $\sim$6 mJ for the $Ne-Kr-F_2$ mixture at a total pressure of 1.6 – 3.2 atm. The maximum efficiency of the laser is $\sim$1.4 %. An original optical technique is worked out for measuring the gas velocity in the working gap. The maximum gas velocity in the gap between the electrodes is found to be 19 m s^{-1} in the experiments. The average output power of the laser for a pulse repetition rate of 3 – 4 kHz is $\sim$12 W, while the relative rms deviation of the laser pulse energy lies in the range 2 % – 3.8 %. It is shown that the refractive index gradient of the active medium, which is related to the free electron concentration in the discharge plasma, plays a significant role in the formation of laser radiation field in the resonator. The characteristic value of the refractive index gradient is found to be no less than 10^{-5} cm^{-1} for the KrF laser wavelength.**

Keywords: *electric-discharge KrF laser, electrode plates, inductive – capacitive stabilisation, pulse repetition rate, emission energy stability, optical inhomogeneities.*

1. Introduction

Excimer lasers with a pulse repetition rate $f \geqslant 4$ kHz used in technological applications have been developed extensively in recent years. Leading manufacturers of ArF(KrF) lasers for UV lithography like Cymer [1], Komatsu [2], and Lambda Physik [3] produce excimer lasers with $f = 4$ kHz and are engaged in research aimed at increasing the pulse repetition rate to 6 – 8 kHz and at enhancing their output energy stability.

A KrF laser pulse repetition rate $f = 4 - 5$ kHz was realised in [4] for a gas circulation velocity $V \approx 55$ m s^{-1} in the electrode gap. Increasing the circulation velocity further by a factor of 1.5 – 2 for achieving an even higher pulse repetition rate is a quite complicated problem. A pulse repetition rate $f = 4$ kHz for the XeF laser was obtained in [5] for $V \leqslant 20$ m s^{-1}. This result was achieved by using a multisectional electrode plate assembly [6] that provided an extremely narrow discharge and its inductive – capacitive stabilisation.

The aim of this paper is to study a KrF laser with a pulse repetition rate up to 4 kHz in such an electrode plate assembly for moderate gas-mixture-circulation velocities (16 – 19 m s^{-1}).

A.V. Andramanov, S.A. Kabaev, B.V. Lazhintsev, V.A. Nor-Arevyan, A.V. Pisetskaya, V.D. Selemir Russian Federal Nuclear Centre, All-Russian Scientific Institute of Experimental Physics, prosp. Mira 37, 607190 Sarov, Nizhegorodskii region, Russia; Tel.: (83130) 45584; Fax: (83130) 45384; e-mail: Lazhintsev@ntc.vniief.ru; web-site: http://www.vniief.ru

Received 23 August 2005
Kvantovaya Elektronika **36** (2) 101 – 105 (2006)
Translated by Ram Wadhwa

2. Experimental results

The KrF laser was constructed on the basis of the working chamber of a CL-5000 commercial excimer laser (Physical Instrumentation Centre, General Physics Institute, Russian Academy of Sciences, Troitsk) and a new electrode assembly with a multisectional discharge gap described in [5]. The height and total length of the discharge gap formed by 25 pairs of anode – cathode plates were 12 and 260 mm, respectively. Preionisation was performed by 25 spark discharges located on one side of the discharge gap (downstream). The 50-cm-long optical cavity was formed by dielectric mirrors ($R_1 = 100$ %, $R_2 = 30$ %) on plane – parallel CaF_2 substrates. The mirrors were arranged in such a way that their dielectric coatings were situated outside the working chamber.

The pulsed pump circuit of the laser contained a storage capacitor C_s (2.8 nF), a peaking capacitor C_p (2.35 nF), and a preionisation capacitor C_{pr} (0.5 nF). The storage capacitor was charged for 240 μs with the help of a resonance-diode circuit. Switching of the storage capacitor in the C – C circuit with the help of a thyratron TGI-1000/25 results in charging of the peaking capacitor. To achieve inductive – capacitive decoupling, a peaking capacitor $C_p^{(i)}$ (0.094 nF) was attached to each pair of electrode plates. Each peaking capacitor was charged from the common storage capacitor through its own decoupling inductance ($L_d^{(i)} = 1$ μH).

Measurement of the gas flow velocity in the discharge gap with electrode plates is a rather difficult problem. At a distance of 0.5 mm above and below the axial line of the electrode system, the gas-flow cross section varied in height by a factor of 1.5 – 2, which caused a strong turbulence in the flow and a nonuniform gas velocity in the discharge gap. In this connection, we used a nonconventional method for measuring the gas flow velocity.

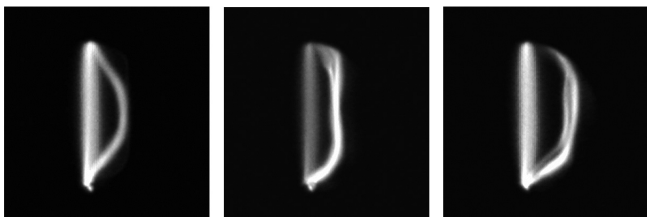

1.5 kHz, 6 V, 4.7 m s^{-1} | 5 kHz, 16 V, 11.6 m s^{-1} | 5 kHz, 28 V, 18.8 m s^{-1}

Figure 1. Characteristic photographs of two discharges for various values of the pulse repetition rate, voltage supplied to the diametrical fan motor, and gas velocity.

This method is based on photographing of two successive discharges on the same frame during gas mixture circulation. Figure 1 shows typical photographs of the discharge glow region.

All the frames clearly show two discharges. The first discharge occurs in the unperturbed active medium (vertical plasma formations), while the second discharge occurs in the medium perturbed by the preceding discharge and displaced downstream. The maximum displacement of the second discharge is observed in the central part of the discharge gap. The gas flow velocity is determined by the magnitude of maximum displacement.

Figure 2 shows the results of experimental measurements. One can see that the gas velocity in the discharge gap depends weakly on the neon pressure. For a neon pressure of 2000 Torr and a voltage exceeding 23 V applied to the motor, the fan operation is disrupted. For a voltage of 28 V across the motor, the magnetic clutch stops imparting torque to the diametrical fan even for a neon pressure of $\sim$1300 Torr. Note that the technique used in the experiments for the gas velocity measurement may ensure an acceptable accuracy of measurements only during the formation of a narrow discharge. The gas flow velocity measured by using this technique is limited by the laser pulse repetition rate.

The laser pulse energy was measured with an ORIEL No 70263 thermocouple head having a time constant $\sim$2.5 s. To improve the accuracy of measurements, the energy of a packet of ten laser pulses was recorded. The gas velocity V in the electrode gap was 8 m s^{-1}, while the pulse repetition rate f was 80 Hz. The laser energy did not decrease from pulse to pulse for such a repetition rate.

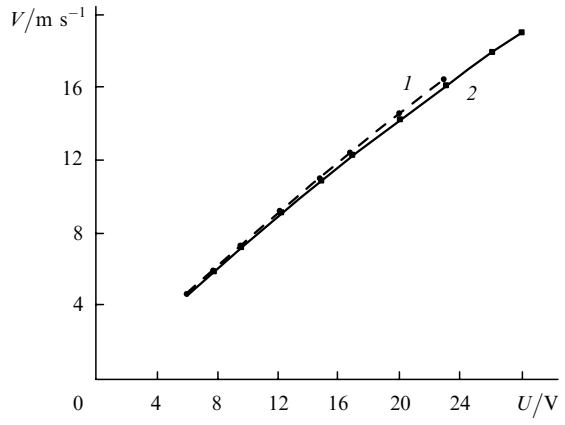

Figure 2. Dependence of the gas velocity V in the electrode gap on the voltage U supplied to the fan motor for gas mixtures F_2:Kr:He:Ne = 4.5:60:85.5:2000 Torr [curve (*1*)] and 4.5:60:85.5:1100 Torr [curve (*2*)] for a storage capacitor charging voltage $U_0 = 14$ kV.

We used Kr–F_2–Ne(He) as the active medium in experiments. The pressure of F_2 and Kr varied in the range 3–4.5 and 40–80 Torr, respectively. Experiments were mainly performed using Ne as the buffer gas since the lasing energy was about 1.6 times lower if He was used for this purpose. The total pressure of the active medium did not exceed 3.2 atm.

The dependence of laser energy on the buffer gas pressure in the active medium was mainly determined by the voltage pulse rise time in the discharge gap. The rise time was increased by including an additional inductance $L_{ad} = 1.12$ μH in the thyratron circuit. In this version of the laser, the duration of charging of peaking capacitors was doubled and amounted to $\sim$120 ns.

Figure 3 shows the results of experiments on optimisation of Ne pressure in the active medium of the KrF laser. For the shortest duration of the pulse front, the maximum laser pulse energy for a charging voltage $U_0 = 20$ kV was 5.7 mJ (the storage energy efficiency was $\eta \approx 1$ %) at the neon pressure $p_{Ne} \approx 1.1$ kTorr [curve (*1*)] and 6.2 mJ ($\eta \approx 1.1$ %) at $p_{Ne} \approx 2$ kTorr [curve (*3*)]. In the latter case, maximum efficiency $\eta \approx 1.4$ % was achieved for $U_0 = 14$ kV. A higher efficiency of the KrF laser with the additional inductance was achieved mainly due to lower losses in the thyratron during switching of the storage capacitor.

The next stage of investigations was associated with the high-frequency regime of laser operation. The energy of a packet of laser pulses (100 or 1000) was measured for a high pulse repetition rate ($f \geqslant 0.5$ kHz) using a thermocouple head. The laser pulse energy stability was studied using a relative pulse energy meter attached to a PC. The device made it possible to register the energy of each pulse (in relative units) for $f \leqslant 5$ kHz. The largest number of pulses registered by the energy meter was 1000.

Figure 4 shows the dynamics of variation of KrF laser energy for various pulse repetition rates. One can see from Fig. 4a that the lasing energy decreases for the first 500 pulses and is virtually stabilised for the subsequent pulses. The lasing energy decreases substantially upon an increase in the pulse repetition rate and for $f = 4$ kHz amounts to just 60 % of the laser pulse energy for low repetition rates in the steady segment (after the first 500 pulses). A similar

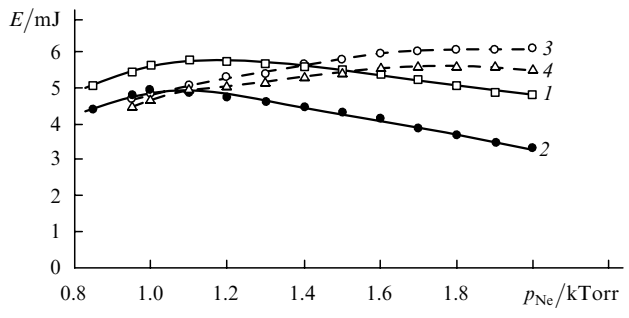

Figure 3. Dependence of the laser pulse energy E on the neon pressure p_{Ne} in the mixture F_2:Kr:He = 4.5:60:85.5 Torr for $U_0 = 20$ kV [curves (*1*) and (*3*)] and 18 kV [curves (*2*) and (*4*)]. Curves (*3*) and (*4*) were obtained using an additional inductance $L_{ad} = 1.12$ μH in the thyratron circuit.

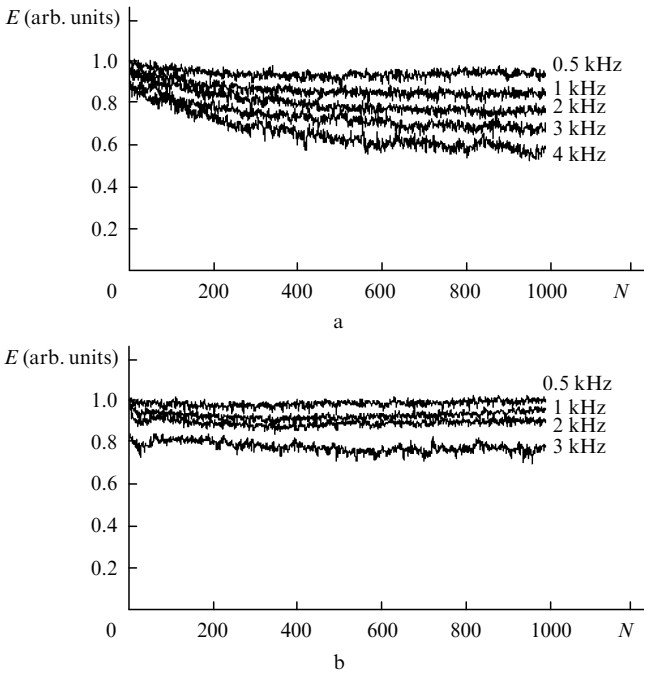

Figure 4. Dependence of the laser pulse energy E on the pulse number N for various values of the pulse repetition rate and mixtures $F_2:Kr:He:Ne = 3:60:57:950$ Torr (a) and $4.5:60:85.5:2000$ Torr (b) for $U_0 = 20$ kV. Curves in Fig. b were obtained using an additional inductance $L_{ad} = 1.12$ μH in the thyratron circuit.

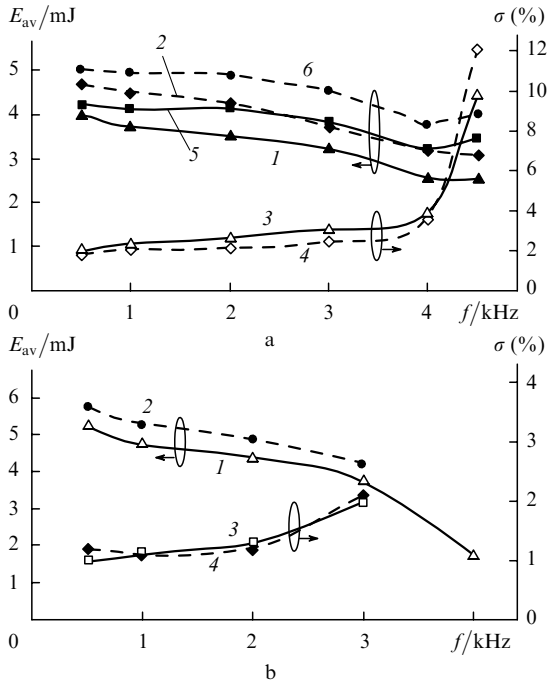

Figure 5. Dependence $E_{av}(f)$ for packets of 1000 [curves (*1*) and (*2*)] and 100 pulses [curves (*5*) and (*6*)], and the dependence $\sigma(f)$ [curves (*3*) and (*4*)] for active mixtures $F_2:Kr:He:Ne = 4.5:60:85.5:1100$ Torr (a) and $4.5:60:85.5:2000$ Torr (b) for $U_0 = 18$ kV [curves (*1*), (*3*) and (*5*)] and 20 kV [curves (*2*), (*4*) and (*6*)]. Curves in Fig. b were obtained using an additional inductance $L_{ad} = 1.12$ μH in the thyratron circuit.

dependence of the laser pulse energy was reported in [4], but the decrease was much smaller: for $f = 4$ kHz, the energy was ~80 % of the lasing energy in the mode with a low pulse repetition rate. Note that the decrease in the lasing energy reported in [4] is due to the formation of products adversely affecting the lasing efficiency. The extent to which this effect is manifested depends on the duration of passive and active passivation of the working chamber, as well as the materials used for its construction. It can be seen from Fig. 4b that the dependence of the lasing energy on the pulse number is quite different in the regime with the additional inductance. A decrease in energy is observed for the first few dozen pulses, while the smooth decrease observed for the subsequent pulses is eventually terminated. For $f = 0.5$–2 kHz, even a slight increase in the pulse energy is observed. Thus, the dynamics of variation of the KrF laser energy from pulse to pulse and the factors responsible for it are apparently more complex than in [4].

The relative rms deviation σ of the output energy from pulse to pulse was calculated for each pulse packet consisting of 1000 pulses. Figure 5 shows the rms deviation σ and the average laser pulse energy E_{av} for packets of 100 and 1000 laser pulses for a repetition rate $f = 0.5 - 4.5$ kHz. The average laser energy for a repetition rate $f = 4$ kHz for the first 100 and 1000 pulses was 3.75 and 3.2 J (Fig. 5a), while the average laser power was 15 and 13 W, respectively. At the steady segment (after the first 500 pulses), the average laser power was even lower (~12 W). For the version with an additional inductance in the thyratron circuit (Fig. 5b), the laser power averaged over 1000 pulses for $f = 3$ kHz was 12.6 W.

One can see from Fig. 5a that the rms deviation σ increases almost linearly from ~2 % for $f = 0.5$ kHz to ~4 % for $f = 4$ kHz and more sharply (to 10 % – 12 %) for $f = 4.5$ kHz (at a gas circulation velocity of 19 m s^{-1}).

For the laser version with an additional inductance (Fig. 5b), the rms deviation was $\sigma = 1\,\%$–$2\,\%$ in the frequency range $f = 0.5 - 3$ kHz, but increased rapidly afterwards (to ~50 %) for $f = 4$ kHz. This is primarily due to a low gas velocity in the electrode gap ($V \leqslant 16$ m s^{-1}). The experimental values of σ are slightly lower than those obtained in [4] for KrF laser with spark preionisation. It should be noted that such a stability of laser pulse energy was attained in [4] for an upstream arrangement of the preionisation sparks, while a breakdown of the frequency mode was observed when the sparks were on the other side of the discharge gap.

The KrF laser beam was visualised by using a luminophore. When the luminophore was placed in the beam, the beam splitting was observed, which was most pronounced when the lasing threshold was slightly exceeded. Figure 6a shows a photograph of the luminophore emission excited by a KrF laser. The luminophore was placed at a distance of 2 m from the output laser mirror. One can see that the radiation power density decreases in the central part of the laser beam. The laser-beam splitting was not eliminated after the adjustment of resonator mirrors.

This effect is even more pronounced for the red emission line ($\lambda = 624 - 755$ nm) of atomic fluorine when the working chamber is filled with a mixture of helium and fluorine (Fig. 6b). Apparently, this effect is due to a high inhomogeneity of the specific pump power in the active laser medium, which leads to a considerable refractive index gradient associated with the nonuniform free electron concentration in the discharge plasma. The change Δn in the refractive index of the active medium of an excimer XeCl laser associated with free electrons in the plasma was

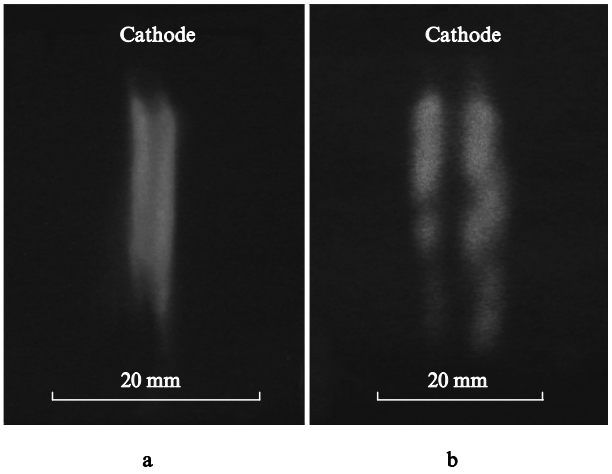

Figure 6. Photographs of transverse laser beam cross sections for a KrF laser (a) and an atomic fluorine laser (b) at a distance of 2 m from the output cavity mirror.

studied, among others, in [7] using the interference technique.

Optical perturbations of the active medium of a KrF laser were investigated using the He–Ne laser probe beam at 633 nm. The experimental setup is shown schematically in Fig. 7. Radiation from He–Ne laser (*1*) passed through diaphragm (*2*) of diameter 1.3 mm and the central part of the discharge gap along the optical axis. It was then focused by lens (*6*) at the endface of optical fibre (*7*) with a diameter 0.8 mm, and the radiation emerging from the optical fibre was registered using photodiode (*8*) and the TDS 3054 oscillograph.

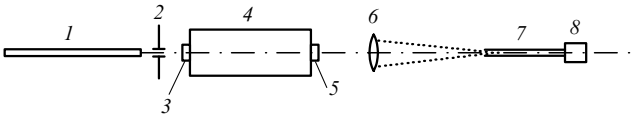

Figure 7. Optical scheme of the experimental setup for studying optical perturbations of the active medium: (*1*) He–Ne laser; (*2*) diaphragm; (*3*, *5*) cavity mirrors; (*4*) working chamber; (*6*) lens ($F = 56$ cm); (*7*) optical fibre; (*8*) photodiode.

The divergence θ of the He–Ne laser beam passing through diaphragm (*2*) was $\sim 1.3 \times 10^{-3}$ rad, the laser spot at the optical fibre had a diameter $d_s \approx F\theta = 0.73$ mm, where F is the focal length of lens (*6*). Figure 8 shows the evolution of optical inhomogeneities in the active medium of the KrF laser. Figure 8a show the laser pulse $P(t)$ sand the voltage pulses $U(t)$ across the peaking capacitor for time referencing of the He–Ne laser radiation intensity (I_1, I_2, I_3) registered by photodiode (*8*).

One can see from Fig 8a [curve (*1*)] that the He–Ne laser radiation intensity $I_1(t)$ incident at the endface of the optical fibre starts decreasing after the beginning of the discharge current pulse from 1 to 0.4, after which it increases with decreasing current. The beginning of the current pulse coincides with the instant of rapid voltage drop across the discharge gap [curve (*4*)]. This is followed by another couple of He–Ne laser radiation intensity drops corresponding apparently to the second and third half-wave discharge current pulses. Considerable technical difficulties

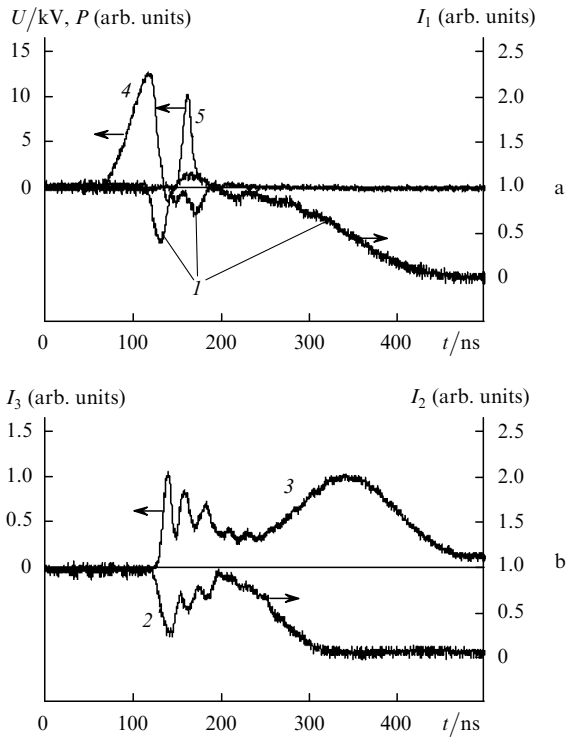

Figure 8. Time dependences of I_1 [curve (*1*)], U [curve (*4*)], and P [curve (*5*)] for the mixture F_2 : Kr : He : Ne = 3 : 60 : 57 : 950 Torr (a) and of I_2 [curve (*2*)], I_3 [curve (*3*)] for the mixture F_2 : Kr : He = 5 : 90 : 690 Torr (b) for $U_0 = 17$ kV.

are encountered in direct measurement of the discharge current pulse in our laser chamber. Such a behaviour of the signal from the photodetector can be attributed to the formation of a diverging cylindrical lens in the active volume due to a concentration gradient for free electrons in the plasma. After $t_1 \approx 100$ ns following the onset of the discharge, the free electron concentration gradient becomes insignificant, while the variation of the active medium refractive index during the next time interval $t_2 \approx 200$ ns is determined by optical gas-dynamic inhomogeneities arising as a result of expansion of the active volume region heated by the discharge and the change in the gas density in this volume. As a result, the He–Ne laser radiation virtually does not fall on the endface of the optical fibre and the signal amplitude I_1 (see Fig. 8a) becomes close to zero. The signal I_1 reappears only when the heated laser medium volume is replaced by the gas flowing from the region of the probe beam.

For the helium mixture, the development time of gas-dynamic optical inhomogeneities $t_2 \approx 100$ ns [curve (*2*) in Fig. 8b], i.e., about half its value in the neon mixture [curve (*1*) in Fig. 8a]. This is due to the fact that the velocity of sound in helium is 2.2 times higher than in neon. Curve (*3*) in Fig. 8b was obtained for the case when the endface of the optical fibre was displaced in the horizontal plane by a distance $\delta \approx 0.8$ mm so that the He–Ne laser radiation does not fall on it until the appearance of optical inhomogeneities and the scattered radiation intensity I_3 is the highest. The appearance of optical inhomogeneities can be clearly seen in the active volume of a cylindrical lens associated with the free electron concentration gradient and density of the active medium. It follows from the experimental results that optical gas-dynamic inhomogeneities appear in the neon

(helium)-based active medium much later than the optical inhomogeneities associated with the free electron concentration, hence their role in the formation of radiation field in the KrF-laser cavity is insignificant.

The obtained results can be used for estimating the refractive index gradient of the active medium for He–Ne laser radiation using the formula $L\mathrm{grad}\, n_{\mathrm{He-Ne}} \approx \delta/F$, where $L = 25$ cm is the length of the active region, $F = 56$ cm, and $\delta \approx 0.08$ cm. We find from this that $\mathrm{grad}\, n_{\mathrm{He-Ne}} \approx 5.7 \times 10^{-5}$ cm^{-1}. The refractive index n_e of the active medium associated with the free electron concentration can be calculated using the formula $n_e = -4.46 \times 10^{-14}\lambda^2 N_e$ [8], where λ is the laser radiation wavelength in cm and N_e is the electron concentration in cm^{-3}. For the KrF laser radiation wavelength ($\lambda = 248$ nm), the refractive index gradient in the active medium $\mathrm{grad}\, n_{\mathrm{KrF}} \approx 5.7 \times 10^{-5}(\lambda_{\mathrm{KrF}}/\lambda_{\mathrm{He-Ne}})^2 \approx 0.88 \times 10^{-5}$ cm^{-1}. Considering that the discharge width $d \approx 0.1$ cm, we obtain the refractive index variation $\Delta n \approx |n_e| \approx d\,\mathrm{grad}\, n_{\mathrm{He-Ne}}/2 = 2.85 \times 10^{-6}$. Accordingly, the maximum electron density N_e in the discharge plasma is $N_e = \Delta n/(4.46 \times 10^{-14}\lambda^2) \approx 1.6 \times 10^{16}$ cm^{-3}.

Thus, the use of a small-width ($\sim$1 mm) discharge and a high specific pump power ($\sim$9 MW cm^{-3}) leads to the formation of a considerable refractive index gradient ($\sim 10^{-5}$ cm^{-1}) in the active medium of the KrF laser. By tilting the electrode plates at a small angle to the optical axis of the laser [6] and increasing the laser beam width in this way, we can considerably lower the impact of this effect on the radiation field formation in the cavity, reduce the beam load on the optical elements and practically preserve the small discharge width in the direction of the gas flow.

3. Conclusions

Our investigations show that the formation of a narrow ($d \approx 1$ mm) discharge in a KrF laser together with its inductive-capacitive stabilisation makes it possible to realise a pulse repetition rate up to 4 kHz for a low velocity of gas circulation (19 m s^{-1}). The rms deviation σ of the radiation pulse energy does not exceed 4 %. An increase in the peaking capacitor charging time to 120 ns increases the optimal pressure of the active medium to $\sim$2 kTorr, while the radiation pulse energy stability improves ($\sigma \approx 1\,\%$–$2\,\%$) in the pulse repetition range 0.5–3 kHz.

It is shown for the first time that a refractive index gradient $n_{\mathrm{KrF}} \approx 10^{-5}$ cm^{-1} associated with the free electron concentration inhomogeneities in the plasma discharge is formed in the active medium of the KrF laser for a narrow discharge and a high specific pump power ($\sim$9 MW cm^{-3}). The emergence of optical inhomogeneities in excimer lasers with a narrow discharge considerably affects the radiation field formation in the laser cavity. A method is proposed for eliminating the negative effect of the 'electron' lens on the excimer laser parameters by using an electrode assembly based on electrode plates tilted at a small angle to the optical axis of the laser.

References

1. Saito T., Sazuki T., Yoshino M., Wakabagashi O., Matsunaga T., Fujimoto J., Kakizaki K., Yamazaki T., Inoue T., Terashima K., Enami T., Inoue H., Sumitani A., Tomaru H., Mizoguchi H. *Proc. SPIE Int. Soc. Opt. Eng.*, **5040**, 1704 (2003).
2. Hueber J.M., Besaucele H., Das P., Eis R., et al. *Proc. SPIE Int. Soc. Opt. Eng.*, **4000**, 1418 (2000).
3. Stamm U., Patzel R., Bragin I., Kleinscmidt J., Lokai P., et al. *Proc. SPIE Int. Soc. Opt. Eng.*, **4000**, 1390 (2000).
4. Borisov V.M., Vinokhodov A.Yu., Vodchits V.A., Eltsov A.V., Ivanov A.S. *Kvantovaya Elektron.*, **30**, 783 (2000) [*Quantum Electron.*, **30**, 783 (2000)].
5. Andramanov A.V., Kabaev S.A., Lazhintsev B.V., Nor-Arevyan V.A., Selemir V.D. *Kvantovaya Elektron.*, **35**, 311 (2005) [*Quantum Electron.*, **35**, 311 (2005)].
6. Andramanov A.V., Kabaev S.A., Lazhintsev B.V., Nor-Arevyan V.A., Selemir V.D. Russian Patent No. 2244990 dated 10.04.03; *Bull. Izobr.*, No. 2, 610 (2005).
7. Borovkov V.V., Andramanov A.V., Voronov S.L. *Kvantovaya Elektron.*, **26**, 19 (1999) [*Quantum Electron.*, **29**, 19 (1999)].
8. Reizer Yu.P. *Gas Discharge Physics* (New York: Springer Verlag, 1997; Moscow: Nauka, 1987).